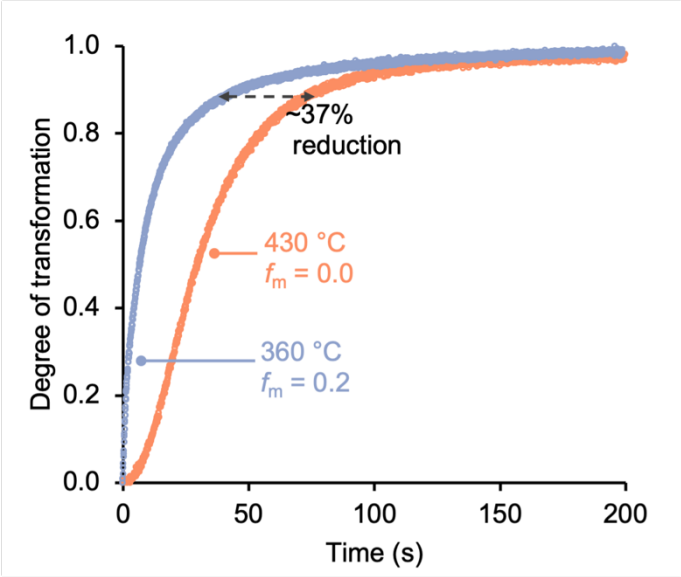

Supplementary Figure 1. Kinetics of bainite formation of a Fe-0.24C-1.3Mn-1.5Si-0.6Cr-0.2Mo-0.02Ti-0.0003B wt.% steel (3B), with f_m indicating the fraction of prior martensite. The degree of transformation is calculated as the instantaneous fraction of bainite divided by the fraction of bainite at stasis. By forming bainite in the presence of martensite (ii), there is a 37% reduction in the time needed to achieve a degree of transformation of 0.9.

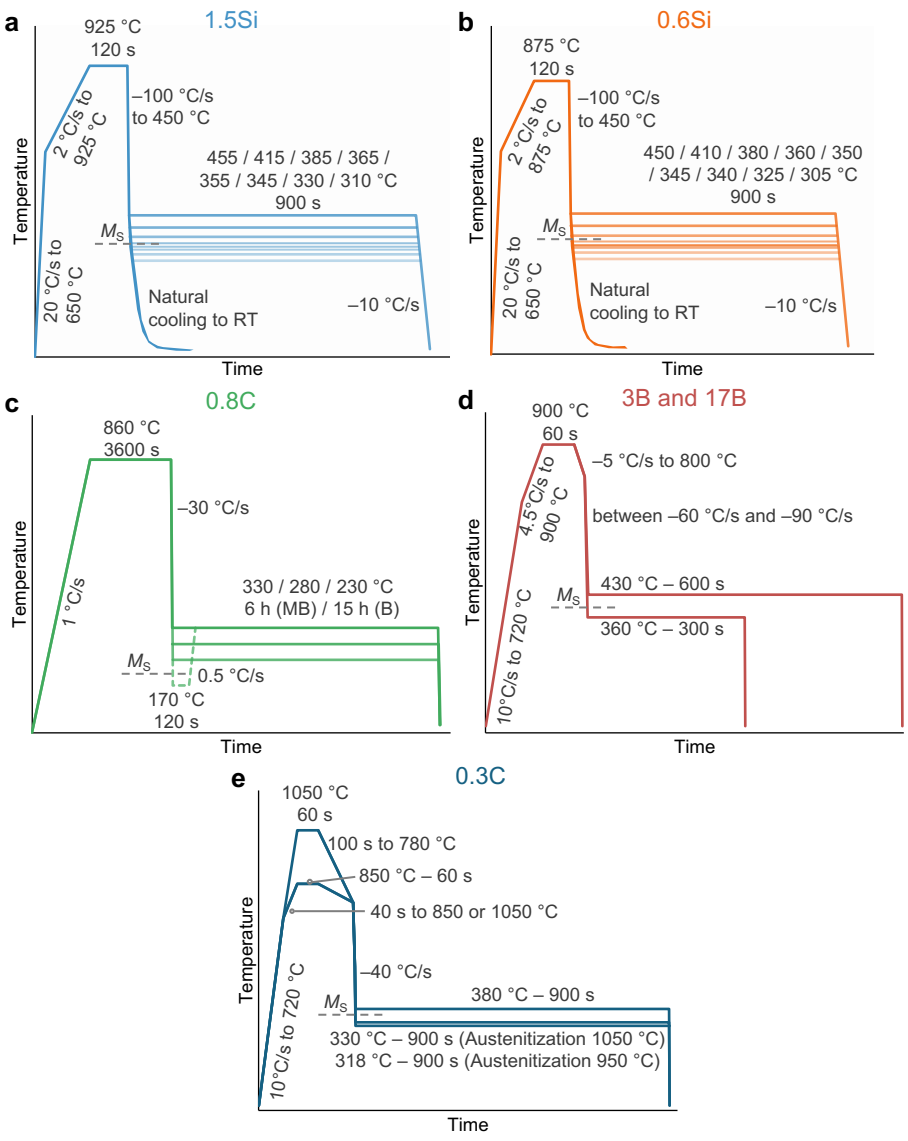

Supplementary Figure 2. Heat treatments applied to steels a, 1.5Si, **b**, 0.6Si, **c,** 0.8C, **d,** 3B and 17B, and **e,** 0.3C. In **c**, solid lines represent the treatment in which bainite formation took place without prior martensite, and dashed lines represent the treatment in which martensite was formed prior to bainite formation.

Supplementary Note 1

According to Olson and Cohen's theory of thermally activated martensite nucleation[1], which is also utilized to explain bainite nucleation[2], the activation energy for nucleation, Q, is

$$Q = Q_0 + \left(\tau_\mu + \frac{\rho_A}{b} E^{str} + \frac{2\sigma}{n_P b}\right) V^* + \left(\frac{\rho_A}{b} V^*\right) \Delta G^{chem}, \quad \text{(S1)}$$

where Q_0 is the activation energy for overcoming the short-range barriers to dislocation movement (e.g. solute atoms), τ_μ is the athermal resistance to dislocation movement, ρ_A is the number of atoms per unit area of the closed packed plane, b is the magnitude of the Burgers vector, E^{str} is the strain energy, σ is the bainite nucleus interfacial energy, n_P is the number of atomic planes of the embryo, V^* is the activation volume, and ΔG^{chem} is the maximum driving force for bainitic ferrite nucleation considering redistribution of carbon between bainitic ferrite and austenite.

Nucleation takes place at arrays of dislocations existing at or near interfaces such as austenite grain boundaries, bainite/austenite interfaces or martensite/austenite interfaces. Given the different characteristics of these boundaries and interfaces, the activation energy is different for each site. The sites can differ in their elemental segregation (which affects ΔG^{chem}), interfacial energy (which affects σ), stress state (which affects E^{str}), and the size of the defects (which affects n_P and V^*).

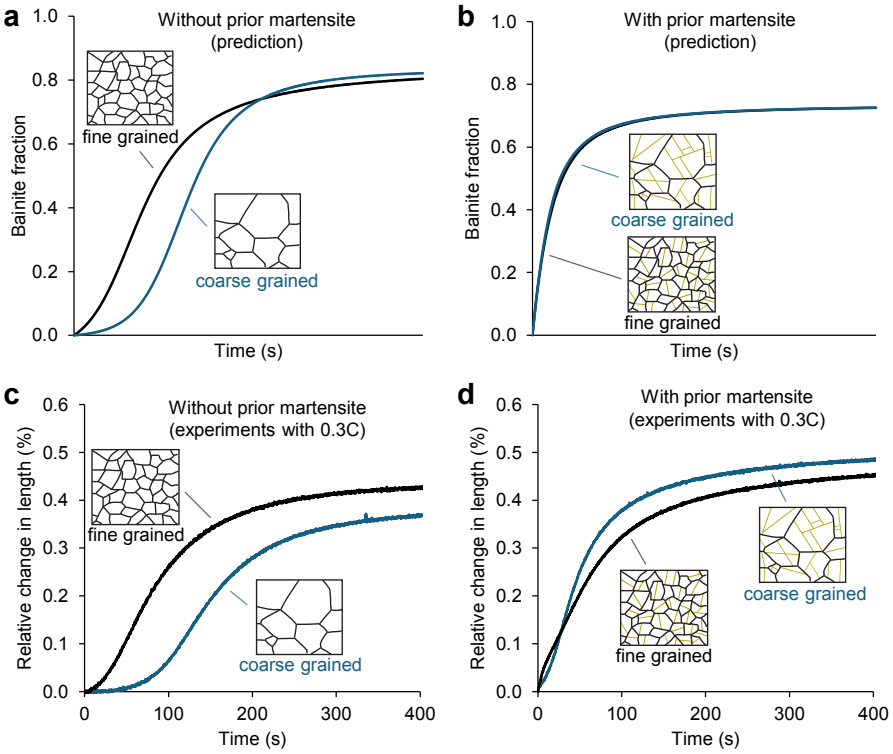

Supplementary Figure 3. Effect of prior austenite grain size on the kinetics of bainite formation. a, b, Simulations using the parameters of steel 1.5Si as the basis for fine grained steel. Curves without prior martensite (**a**) were simulated at 415 °C, and curves with prior martensite (**b**) at 345 °C, with 0.20 volume fraction of prior martensite. The fine grained steel has a PAGS of 13 µm, and the coarse grained steel of 100 µm. **c, d,** Experimentally measured effect of PAGS for steel 0.3C (Fe-0.30C-1.3Mn-1.5Si-0.6Cr), with the coarse grained sample austenitized at a higher temperature (1050 °C) than the fine grained sample (850 °C). **c** shows curves at 380 °C, which is above M_S. **d** shows curves at 318 °C for the fine grained steel and 330 °C for the coarse grained steel. In both cases, a volume fraction of around 0.10 of prior martensite is present. Different holding temperatures were used because changing the PAGS changes the M_S of the steel, and if the same holding temperature was used for both steels, they would have different fractions of martensite. The temperature difference might be the reason for the slight difference in the kinetics between the fine and coarse grained steels.

Supplementary Note 2

A theoretical estimate of S_{MA} can be derived by considering that bainite nucleates at the broad faces of martensite laths or plates. The surface area of the broad face per volume of martensite, S_{M}, can be calculated as $2/t_{\mathrm{m}}$, where t_{m} is the thickness of the martensite laths or plates. To calculate S_{MA}, it is also necessary to know the distribution of martensite within austenite grains. Although it is known that at the end of the transformation martensite is organized into packets and blocks, the initial sequence of martensite formation is less understood because it is experimentally difficult to observe. A reasonable approximation is that during the initial stage laths or plates of martensite grow in different crystallographic directions inside austenite grains, and during the final stage martensite forms in the untransformed region as parallel laths or plates. This sequence of formation was proposed by Raghavan, McMurtrie, and Magee[3,4] and has some experimental support in the work of Nambu et al.[5]. During the initial stage of martensite formation, S_{MA} can then be approximated by Eq. (S2)

$$S_{\mathrm{MA}} = S_{\mathrm{M}} f_{\mathrm{m}} f_{\gamma}, \tag{S2}$$

where f_{m} is the fraction of martensite and f_{γ} is the fraction of austenite. By substituting S_{M} for $2/t_{\mathrm{m}}$, Eq. (S2) can be rewritten as

$$\frac{S_{\mathrm{MA}}}{f_{\gamma}} = \frac{2}{t_{\mathrm{m}}} f_{\mathrm{m}}. \tag{S3}$$

Supplementary Figure 4 shows $S_{\mathrm{MA}}/f_{\gamma}$ as a function of martensite fraction for all three steels for martensite fractions up to 0.20. For each steel, a linear curve was fitted, and the slope of such curves were used to calculate the thickness of the martensite lath, t_{m}, using Eq. (S3). Supplementary Table 1 shows the values of t_{m} calculated using Eq. (S3) and using the model for martensite lath thickness developed by Galindo-Nava and Rivera-Díaz-del-Castillo[6], which was validated against experimental measurements of martensite lath thickness.

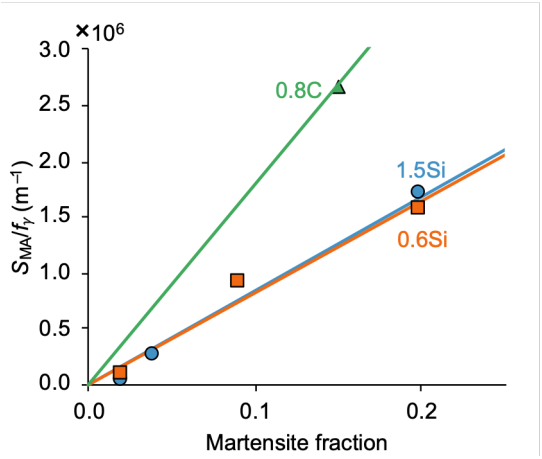

Supplementary Figure 4. Area of M/A interface per volume of remaining austenite as a function of martensite fraction. Markers represent points calculated using the values of S_{MA} found using the analytical model presented here, and solid lines are the best fit linear curves for each steel.

The martensite lath thickness – calculated using the fitted values of S_{MA} – of Steels 1.5Si and 0.6Si are similar, at 0.24 μm on average, while that of Steel 0.8C is finer, at 0.11 μm. This trend is in close agreement with the prediction of Galindo-Nava's model. The thickness calculated using the present model is consistently thicker than the thickness calculated using Galindo-Nava's model. This overestimation is possibly due to the assumption that martensite initially nucleates in different crystallographic directions inside each austenite grain. If some laths or plates nucleate parallel to each other and share a martensite/martensite interface instead of a martensite/austenite interface, Eq. (S2) will overestimate S_{MA} and, consequently, Eq. (S3) will overestimate t_{m}. A correction factor, K_{MM}, can be applied to Eq. (S2) to account for the fraction of parallel martensite laths sharing a martensite-martensite interface, which then becomes

$$S_{\mathrm{MA}} = K_{\mathrm{MM}} S_{\mathrm{M}} f_{\mathrm{m}} f_{\gamma}, \tag{S4}$$

with K_{MM} equal to 0.59 in the case of the steels in Supplementary Table 1 – if the thickness calculated using Galindo-Nava's model is considered to be the true value of the thickness.

Supplementary Table 1. Thickness of martensite laths or plates.

Steel	**Martensite lath or plate thickness (μm)**	
	Calculated from S_{MA}	Calculated from ref. [24]
0.8C	0.112	0.066
1.5Si	0.238	0.143
0.6Si	0.243	0.143

Supplementary Note 3

The approach in Supplementary Note 2 allows to estimate S_{MA} during the initial stage of martensite formation, possibly to fractions up to 0.20, but it overestimates S_{MA} at larger fractions. Nonetheless, a good correlation was found between S_{MA} and the rate of martensite formation for fractions of martensite of up to 0.7, as shown in Figure 3 of the main text.

The kinetics of martensite formation is generally represented by the Koistinen-Marburger (KM) equation[7,8], which can be written as

$$f_m = 1 - \exp[-\alpha_{\mathrm{m}}(T_{\mathrm{KM}} - T)], \tag{S5}$$

where α_{m} is the composition-dependent KM exponent term, T_{KM} is the KM martensite start temperature, which can be around 10 to 30 °C below the experimentally measured M_{S}. While Eq. (S5) can yield a fair estimate of the fraction of martensite for a given temperature, it does not capture the evolution of the rate of martensite formation throughout the transformation.

Magee[9] showed that the Koistinen-Marburger equation can be theoretically derived by assuming the number of nucleation events of martensite laths or plates per available austenite fraction is proportional to the undercooling, that is,

$$\mathrm{d}N = \frac{\mathrm{d}f_{\mathrm{m}}}{\bar{V}} = \varphi(1 - f_{\mathrm{m}})\mathrm{d}(\Delta T), \tag{S6}$$

where N is the number of laths or plates of martensite nucleated, $\bar{V}$ is the average volume of martensite laths or plates, and φ is a proportionality constant value. Following Magee's assumption that $\bar{V}$ is constant throughout most of the transformation, Eq. (S6) can be integrated to yield Eq. (S5).

The assumption in Magee's work, and in the Koistinen-Marburger equation, is that the rate of martensite formation per austenite fraction is constant, which can be represented as

$$\frac{\mathrm{d}f_{\mathrm{m}}}{\mathrm{d}T}\frac{1}{1-f_{\mathrm{m}}} = \alpha_{\mathrm{m}}. \tag{S7}$$

However, Eq. (S7) does not match the experimentally measured kinetics of martensite formation. The rate of martensite formation per available fraction of austenite is not constant, as Supplementary Figure 5 shows. Instead, the rate first increases linearly with martensite fraction, reaches a maximum at a fraction of around 0.20, and then slowly decreases. Therefore Koistinen-Marburger equation, and consequently Magee's theory, only represents the average rate of martensite formation from M_{S} to the quenching temperature. The KM equation and Magee's theory are unable to represent the rate of martensite formation because they do not include the effect of autocatalysis, which is a crucial aspect of martensite formation[10,11].

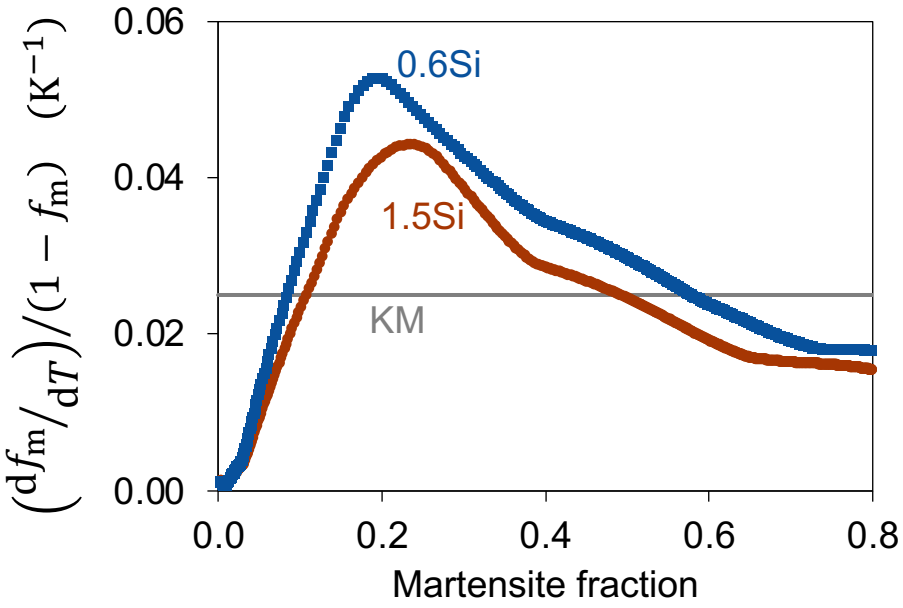

Supplementary Figure 5. Kinetics of athermal martensite formation for steels 0.6Si and 1.5Si measured by dilatometry.

When a martensite lath or plate forms, it deforms the surrounding austenite. The deformation creates defects in the austenite at which more martensite can nucleate, thus creating the autocatalytic effect in martensite formation. Most of the martensite laths or plates nucleate by autocatalysis from these sites that are created during the transformation, not from initially present defects[9,12,13]. To introduce autocatalysis in Magee's theory, the term $\varphi(1-f_\mathrm{m})$ in Eq. (S6) needs to be substituted by the existing number density of potential nucleation sites for martensite. Since the new potential nucleation sites are created in the austenite surrounding the martensite, the number density of these new potential nucleation sites can be considered proportional to the area per volume of the M/A interface. With this modification, Eq. (S6) becomes

$$\mathrm{d}N = \frac{\mathrm{d}f_\mathrm{m}}{\bar{V}} = (\varphi_\mathrm{i} + \varphi_\mathrm{A} S_\mathrm{MA})\mathrm{d}(\Delta T), \tag{S8}$$

where φ_i is the initial value of φ, which is related to the initial potential nucleation sites, and φ_A is a proportionality constant related to the potential nucleation sites created by autocatalysis. Since autocatalysis dominates over the initial nucleation rate even at martensite fractions as low as 0.01 (see the slow initial rate in Supplementary Figure 5, and the works of refs.[9,12,13]), Eq. (S8) can be approximated as

$$\mathrm{d}N = \frac{\mathrm{d}f_\mathrm{m}}{\bar{V}} \approx \varphi_\mathrm{A} S_\mathrm{MA}\mathrm{d}(\Delta T), \tag{S9}$$

and, from Eq. (S9) and following Magee's assumption of approximately constant $\bar{V}$ throughout most of the martensitic transformation,

$$\frac{\mathrm{d}f_\mathrm{m}}{\mathrm{d}T} \approx K S_\mathrm{MA}, \tag{S10}$$

where K is a proportionality constant.

In the main text it was shown that the main parameter controlling the acceleration that martensite induces in bainite formation is the number of new potential nucleation sites created at M/A interfaces. From Eqs. (1) and (4), $\mathrm{d}N_\mathrm{MA}/\mathrm{d}t \propto S_\mathrm{MA}$, which in combination with Eq. (S10) yields

$$\frac{\mathrm{d}f_{\mathrm{m}}}{\mathrm{d}T} \propto \frac{\mathrm{d}N_{\mathrm{MA}}}{\mathrm{d}t}. \tag{S11}$$

Eqs. (S8) to (S11) give the theoretical background for the correlation shown in Figure 3b. Physically, this correlation indicates that when martensite forms, the surrounding austenite is strained, and the defects created (such as dislocations and the M/A interface itself) can act as nucleation sites for bainite and martensite.

Supplementary Note 4

Supplementary Figure 6 compares the kinetics of bainite formation with and without the presence of martensite for steel 1.5Si, 0.6Si, and 0.8C at different isothermal holding temperatures. The y-axis on the graph in Supplementary Figure 6a is the combined fraction of martensite and bainite, and the curve with prior martensite is shifted in time so that it starts from the same point as the curve without prior martensite, as proposed in the work of Smanio and Sourmail[14]. The plot in Supplementary Figure 6a directly compares the accelerating effect of prior martensite with the accelerating effect of an equal fraction of bainite (autocatalysis). In Supplementary Figure 6b, the difference between the curves is plotted.

For Steel 0.8C, the samples were either transformed to bainite directly after austenitization by quenching to the desired temperature of bainite formation (230 to 330 °C) or by quenching to 170 °C to form prior martensite and reheating the desired temperature of bainite formation (230 to 330 °C). This approach allows directly comparing the kinetics of bainite formation with and without the presence of prior martensite. However, for the low carbon steels, bainite was formed in the presence of martensite by a one-step treatment below M_S, and it is not possible to experimentally make the same comparison as for Steel 0.8C. Thus, the model developed in the present work was used to simulate the kinetics of bainite formation without the presence of martensite in treatments below M_S for the low carbon steels.

For the three steels, the acceleration by martensite is stronger at higher temperatures. The difference does not seem to be controlled by the fraction of martensite or

the area of M/A interface. For steel 0.6Si, the difference in acceleration by prior martensite and the autocatalysis in bainite formation is higher at 350 ° than at 345 °C, despite S_{MA} being higher at 345 °C than at 350 °C. For steel 0.8C, S_{MA} is the same regardless of the temperature at which bainite is formed; still, the acceleration is more pronounced at higher temperatures.

Smanio and Sourmail[14] reported that for a 100Cr6 steel the accelerating effect of 0.15 or 0.30 volume fraction of prior martensite was the same as the autocatalytic acceleration from a similar fraction of bainite for bainite formation at 220 and 250 °C. The same effect was observed in steel 0.8C at 280 °C. However, at 230 °C, martensite accelerates less than a similar fraction of bainite; and at 330 °C, it accelerates more. Thus, the effect reported by Smanio and Sourmail is rather a temperature-dependent effect than a general one.

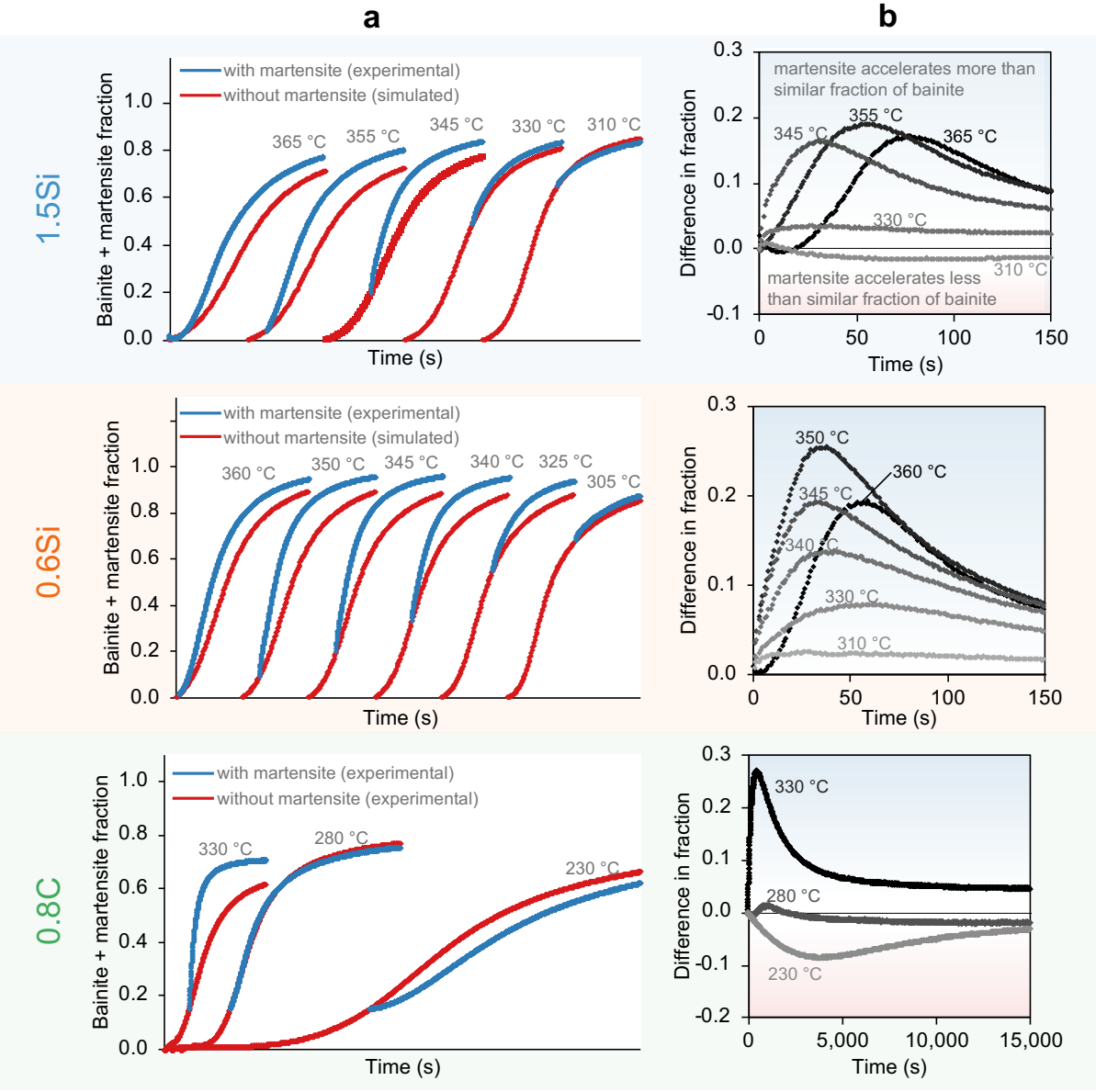

Supplementary Figure 6. Comparison between acceleration by martensite and autocatalysis in bainite formation for steels 1.5Si (top), 0.6Si (middle), and 0.8C (bottom). (a) kinetics of bainite formation with and without prior martensite, with the curves with prior martensite shifted in time to match those without prior martensite. (b) difference between the curves with and without prior martensite.

Supplementary Note 5

To investigate if the more intense acceleration at higher temperatures is an effect intrinsic to the temperature of bainite formation or if it is related to phenomena taking place during martensite tempering (e.g. stress relaxation), we performed an additional experiment with steel 0.8C. In this extra experiment, after quenching to 170 °C, the specimen was heated to 330 °C, held for 10 s, and cooled back down to 230 °C, as shown in Supplementary Figure 7a. The results of the experiment were compared to the results of the treatment in which the steel was heated directly to 230 °C after quenching to 170 °C.

Supplementary Figure 7b shows the relative change in length (RCL) for the two treatments during reheating from the quenching temperature of 170 °C. At around 280 °C, a deviation from linearity indicates that bainite started to form in the steel that was being heated to 330 °C. A volume fraction of 0.05 to 0.10 of bainite was formed during heating to 330 °C and holding for 10 s. Thus, if the higher intensity of acceleration at higher temperatures is due to the aspects that are related to martensite tempering (such as stress relaxation and carbon partitioning away from the M/A interface), then these phenomena have already started taking place during heating to 330 °C. Ribamar et al.[15] studied the stress relief in austenite during tempering of a steel similar in chemical composition to steel 0.8C by *in situ* synchrotron X-ray diffraction. While at 230 °C almost no stress relief had taken place, at around 300 °C a sharp drop in residual stress started taking place.

Supplementary Figure 7c shows that the kinetics of bainite formation during holding at 230 °C is mostly unaffected by reheating to 330 °C. The main difference between the two curves is that the RCL at the end of the treatment is slightly smaller for the sample reheated

to 330 °C, possibly because this sample already had some 0.05 to 0.10 of bainite formed before the start of isothermal holding. Such a result indicates that the stronger acceleration induced by martensite at higher temperatures is related to an intrinsic effect of temperature and not to other aspects such as martensite tempering, redistribution of carbon, or stress relief. According to the results of our model, such intrinsic effect of temperature is related to the effect of temperature on the size of bainite sub-units.

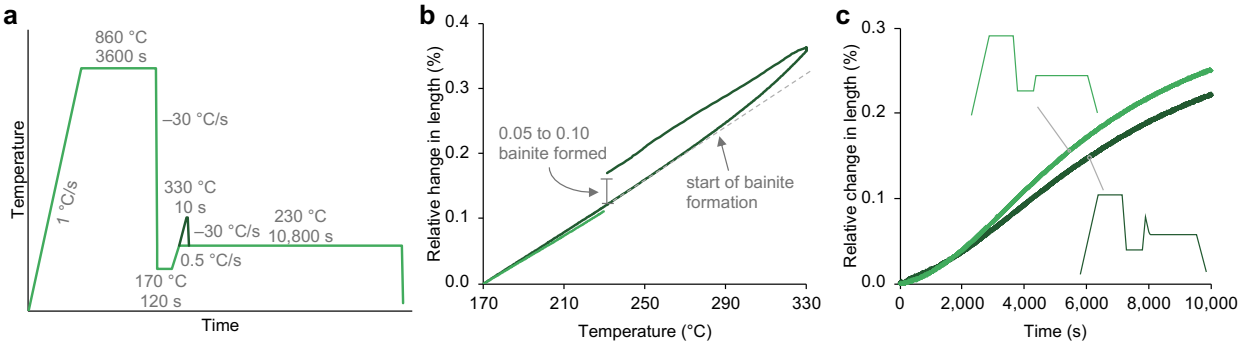

Supplementary Figure 7. Kinetics of bainite formation in the presence of martensite at 230 °C for steel 0.8C with and without an intermediate heating to 330 °C. (a) Time temperature profile of the two treatments. (b) Relative change in length during heating to 230 °C or 330 °C after quenching to 170 °C. (c) Relative change in length during isothermal holding at 230 °C.

Supplementary Note 6

For the low carbon steels, the samples were quenched from the austenitization temperature to an isothermal holding temperature below M_S. Because of its athermal nature, martensite is expected to form only during this quenching. Bainite, on the other hand, is expected to form not during quenching but during isothermal holding, as it is a thermally activated transformation. To distinguish the phase fraction of martensite and bainite, it is therefore important to accurately choose a point in time that marks the transition between quenching and isothermal holding. Before this point, any transformation product is considered martensite. After this point and during holding, any transformation product is considered bainite. This seemingly simple distinction is, in fact, not trivial.

Navarro-López et al.[19] used the temperature measured by a thermocouple welded to the center of the samples to differentiate cooling from isothermal holding. They considered the point zero for the start of bainite formation as the time at which the temperature reached its lowest value during cooling. Following this procedure, they found that prior martensite accelerated the initial nucleation rate of bainite by two orders of magnitude.

The procedure of Navarro-López et al., however, overlooks the thermal gradients present in the dilatometry sample. The thermocouple in the center is used for temperature control, and thus it closely follows the programmed time-temperature profile. On the other hand, the border of the samples, which is in contact with the cold pushrods, is always at a lower temperature than the center[20,21] and is not automatically controlled by the dilatometer. Hence, at the time zero chosen by Navarro-López et al, the border of the sample could still be cooling down and forming martensite.

In the experiments for steel 0.6Si and 1.5Si, in addition to the thermocouple welded to the center of the sample for temperature control, a second thermocouple was welded at approximately 1 mm from the border of the sample. The temperature reading from the second thermocouple was recorded but not used for temperature control. Supplementary Figure 8a shows the temperature at the center and at the border of the sample for steel 1.5Si treated at 345 °C. Time zero is chosen following the procedure of Navarro-López. During the first seconds of isothermal holding, the temperature at the center of the sample is stable; at the border of the sample, the temperature is still decreasing for around 5 seconds, and it cools down to 325 °C. During these 5 seconds, martensite is forming at the border of the sample. The rate of martensite formation can be calculated as:

$$\frac{\mathrm{d}f_{\mathrm{m,border}}}{\mathrm{d}t} = \frac{\mathrm{d}T_{\mathrm{border}}}{\mathrm{d}t}\frac{\mathrm{d}f_{\mathrm{m}}}{\mathrm{d}T}\bigg|_{T_{\mathrm{border}}}, \tag{S12}$$

where $f_{\mathrm{m,border}}$ is the fraction of martensite at the border of the sample and T_{border} is the temperature at the border of the sample. If the average temperature of the sample is estimated to be the average between the temperature at the center (which is constant during isothermal holding) and at the border, the rate of martensite formation during the first seconds of isothermal holding can be estimated as half of the rate calculated from Eq. (S12),

$$\frac{\mathrm{d}f_{\mathrm{m}}}{\mathrm{d}t} \approx \frac{1}{2}\frac{\mathrm{d}f_{\mathrm{m,border}}}{\mathrm{d}t}. \tag{S13}$$

Supplementary Figure 8b shows that the rate of transformation at the beginning of isothermal holding at 345 °C for steel 1.5Si is 0.08 s^{-1}. This rate of transformation is calculated based on the change in length of the sample, ΔL. Since bainite and martensite cause the same change in length, which is dictated by the difference in molar volume between FCC and BCC, the rate of transformation calculated using ΔL is the sum of the rate of bainite and martensite formation. While the experimental rate is 0.08 s^{-1}, the rate of bainite formation calculated from the model is only 0.02 s^{-1}. However, the sum of the rate of bainite formation, calculated from the model, and of martensite formation, calculated using Eq. (S13), matches well the experimental rate of transformation. Therefore, the high initial transformation rate originates from martensite forming at the border of the samples rather than from bainite formation.

To confirm if martensite formation at the border of the sample was also the reason for the extremely high initial transformation rate found by Navarro-López et al., we repeated their experiments using a second thermocouple welded at 1 mm from the border of the sample. The same samples, dilatometer, and parameters from Navarro-López were used. Supplementary Figure 8c shows again that during the first seconds, the temperature is stable at the center of the sample, but it is still cooling down at the border. The temperature at the border took around 12 seconds to stabilize, which is longer than the five seconds for steel 1.5Si. The difference might be because of the different sample geometry (plate vs cylinder) and atmosphere. In the experiments of Navarro-López, a helium atmosphere is kept during the beginning of isothermal holding. For steel 1.5Si, the chamber starts being

pumped after fast cooling to 450 °C. Longitudinal thermal gradients are milder when the dilatometer chamber is under vacuum than when it is filled with helium[21].

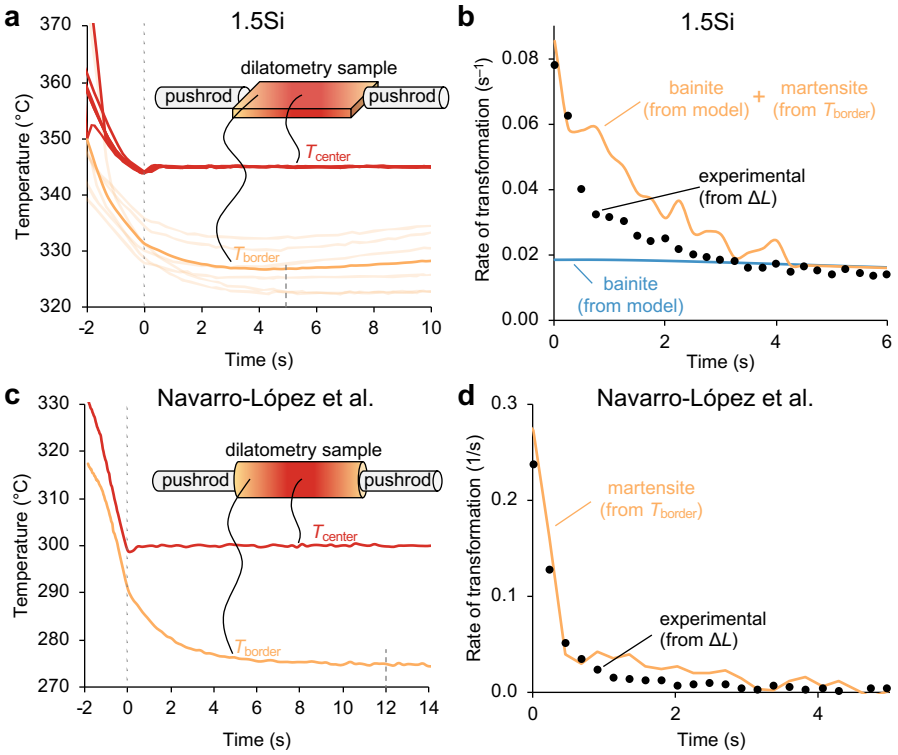

Supplementary Figure 8. Borders of dilatometry samples, which are in contact with cold pushrods, are still cooling during the first seconds of isothermal holding, and thus martensite is still forming and accounts for the high initial rate of transformation. a, c, Temperatures measured by thermocouples welded to the center of the sample and at 1 mm from the border of the sample for steel 1.5Si and the steel used by Navarro-López et al., respectively. **b, d**, Initial rate of transformation (bainite and martensite) calculated using the measured ΔL, rate of martensite formation calculated using Eq. (S13), and rate of bainite formation calculated using the model for steel 1.5Si and the steel used by Navarro-López et al., respectively. For steel 1.5Si, six repetitions of the experiment were made. Three repetitions followed the cooling profile from the Methods section, and the other three had constant cooling rate of 50, 100, and 200 °C/s. All six experiments gave fairly similar results

and are shown in **a** using transparent lines. The solid, opaque lines in **a** and **b** are the average from all six experiments.

The initial rate of transformation for Navarro-López et al.'s steel is 0.23 s^{-1}. Supplementary Figure 8d shows that this high initial rate can be fully accounted for by the martensite formation calculated using Eq. (S13). After 12 seconds, when the temperature at the border is stable, the rate decreases by a factor of 200 to less than 0.001 s^{-1}, which is in the same order of magnitude as for the samples without prior martensite[19,22]. Because the second thermocouple was welded at 1 mm from the border of the sample, it cannot be ruled out that even after 12 seconds the regions closer to the border are still cooling down and a small fraction of martensite is still forming.

The results presented in Supplementary Figure 8 show that the acceleration of bainite nucleation by a factor of two orders of magnitude reported by Navarro-López et al. was, in reality, an overestimation resulting from an artifact of measurement. Such an artifact is inherent to the quenching dilatometers based on induction heating, which are routinely used in scientific and technological works to measure the kinetics of phase transformations. Thus, the incorrect interpretation by Navarro-López et al., used here to illustrate this artifact, might be present in similar studies carried out by other researchers. For instance, Ravi et al.[22] modeled bainite formation at the M/A interface using the high initial nucleation rate, which may be, in reality, mostly martensite formation.

Given this artifact, it is difficult to accurately measure the initial rate of bainite formation and to differentiate martensite and bainite formation. In steels in which bainite formation is slow and a negligible fraction is expected to form in the first 10 to 20 seconds of

isothermal holding, all the transformation that happens during this time can be considered to be martensite. However, that is not the case for steel 1.5Si. The rate of bainite formation is estimated to be around 0.02 s^{-1} during the first seconds of isothermal holding, and thus, in the first 10 seconds, up to 0.20 volume fraction of bainite could be formed. To better differentiate bainite and martensite in this case, it is useful to use the model presented in this work to estimate the rate of bainite formation. The rate of martensite formation can be modeled using an exponential decay type expression, such as the expression Ravi et al. used to model bainite nucleation at the M/A interface[22]. In either case, it is good practice to use a second thermocouple welded to the border of the sample.

Supplementary Note 7

The experimental kinetics of bainite formation for steel 3B at 430 °C (without prior martensite) was used to find the model fitting parameters that were used as the basis for the simulations shown in Figure 5. The extracted values were Q_{AGB} = 241.5 kJ/mol, Q_{BA} = 232.4 kJ/mol, X_{b} = 0.0088 at.fr. (X_{nom} = 0.0109 at.fr.).

The effect of boron was simulated as a 5 KJ/mol increase in the activation energy for grain boundary nucleation (Q_{AGB} = 246.5 kJ/mol), while Q_{BA} and X_{b} were kept constant. The value of 5 KJ/mol was chosen because its effect is qualitatively in line with experimental observations of the ratarding effect of boron on bainite formation kinetics.

From Eq. (S1), the overall contribution of the creation of new interfaces to the activation energy for bainite nucleation is $2\sigma V^*/(n_{\mathrm{P}}b)$, where σ is the average energy of the creation of the new interfaces. Assuming n_{P} equal to 10 atomic planes[1], and V^* equal to 60 atomic volumes of iron[16], a 5 kJ/mol increase in Q would be caused by a 21 mJ/m^2 increase in σ.

Considering that bainite nucleates inside an austenite grain γ_1 at its boundary with austenite grain γ_2, σ can be estimated as

$$\sigma = \frac{\sigma_{\mathrm{B}/\gamma_1} A_{\mathrm{B}/\gamma_1} + \sigma_{\mathrm{B}/\gamma_2} A_{\mathrm{B}/\gamma_2} - \sigma_{\gamma_1/\gamma_2} A_{\mathrm{B}/\gamma_2}}{A_{\mathrm{B}/\gamma_1} + A_{\mathrm{B}/\gamma_2}}, \quad \text{(S14)}$$

where $\sigma_{i/j}$ is the average energy of the i/j interface and $A_{i/j}$ is the area of the i/j interface. In Eq. (S12), the term $\sigma_{\gamma_1/\gamma_2}A_{\mathrm{B}/\gamma_2}$ captures the elimination of part of the γ_1/γ_2 boundary by the bainite nucleus.

Following Prithiv's[17] suggestion that boron alloying decreases $\sigma_{\gamma/\gamma}$ by 170 mJ/m^2, the overall decrease in σ by 21 mJ/m^2 means that A_{B/γ_2} corresponds to 12% of the total interfacial area of the nucleus.

To predict the kinetics of bainite formation at 360 °C with a fraction of prior martensite of 0.20, it is necessary to estimate the values of Q, X_{bm}, and S_{MA}. Following the linear relationship of temperature and activation energies shown in Figure 3, we assumed that Q_{AGB} and Q_{BA} decrease at a rate of 420 J/(mol K). Therefore, at 360 °C, Q_{AGB} was 212.1 kJ/mol for steel 3B and 217.1 kJ/mol for steel 17B, and Q_{BA} was 203.0 kJ/mol for both steels. X_{bm} was assumed to be constant, at 0.0088. The parameters for bainite nucleation at M/A interfaces were assumed to be the same for steels 3B and 17B, given that boron has negligible effect on the formation of martensite[18]. Q_{MA} was assumed to be 207.5 kJ/mol, which is the average of Q_{AGB} and Q_{BA} for steel 3B. The choice of estimating Q_{MA} as the average between Q_{AGB} and Q_{BA} is based on the results of Figure 3. Since steels 3B and 17B have the same carbon content as steels 1.5Si and 0.6Si (0.24 wt.%), S_{MA} was assumed to be 1.25 x 10^6 m^{-1} at f_{m} = 0.20, consistent with the values found for 1.5Si and 0.6Si (Figure 3).

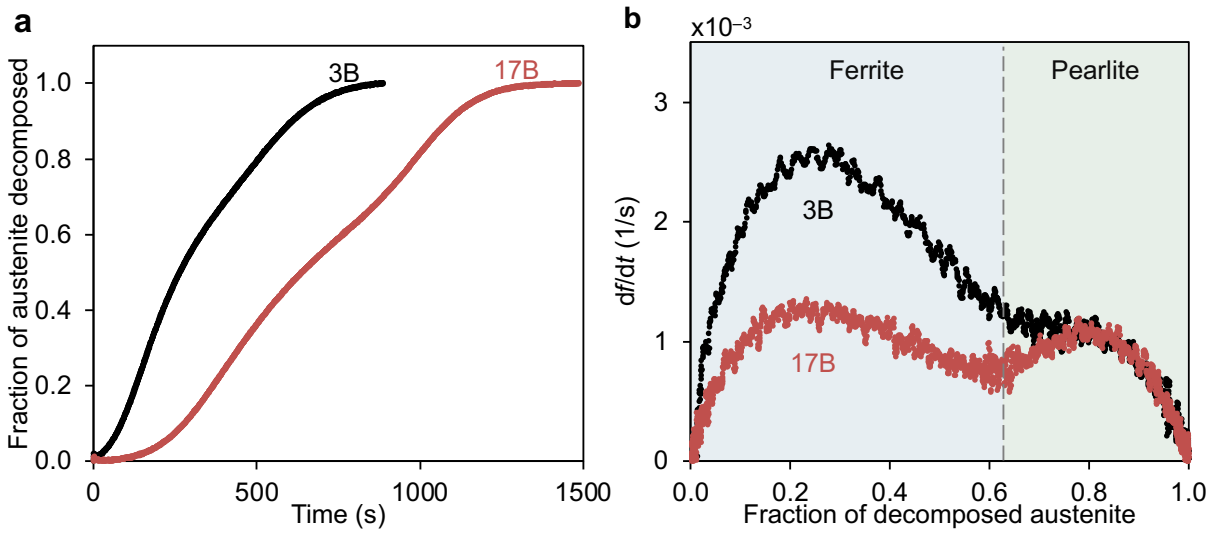

Supplementary Figure 9. Boron addition slows down austenite decomposition into ferrite and pearlite at 650 °C. a, fraction of austenite decomposed as a function of isothermal holding time for steel 3B and 17B. **b**, rate of fraction of austenite decomposed as a function of the fraction of austenite decomposed for steel 3B and 17B. There are two peaks in the rate, with the first being decomposition to proeutectoid ferrite and the second to pearlite. The addition of boron affects only the ferrite formation, since this reaction starts at austenite grain boundaries.

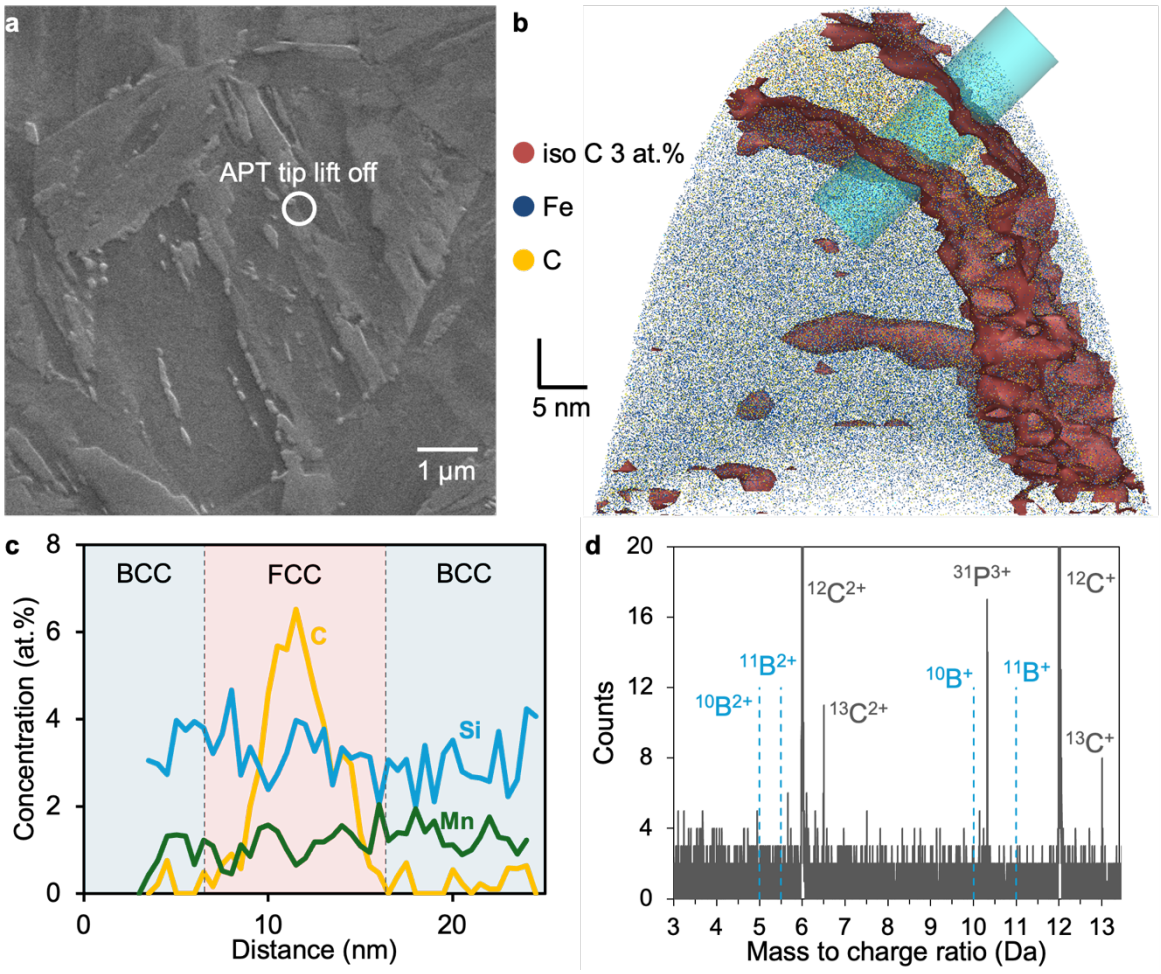

Supplementary Figure 10. APT results showing no boron segregation to BCC/FCC interfaces. a, SEM image of the area from which the APT tip was taken. **b,** 3D map showing the distribution of iron (blue) and carbon (yellow) atoms. Red indicates the isoconcentration surface at 3 at.% of carbon. **c,** Chemical composition along the region of interest delimited by the turquoise cylinder in **b**. **d,** mass to charge ratio of all detected ions showing that no signal coming from boron was detected, indicating that the concentration of boron is 10 ppmw or below, which is the detection limit of this technique. Blue vertical dashed lines indicate the position of possible peaks coming from boron.

Supplementary Note 8

According to the model proposed by Da Rosa et al.[23], based on McLean's segregation equation[24], the excess solute at the austenite grain boundaries, Γ, is calculated as

$$\Gamma = \Gamma_{\max} X \exp\left(-\frac{\Delta G_{\text{seg}}}{k_{\text{B}} T}\right), \quad \text{(S15)}$$

where $\Gamma_{\max}$ is the excess solute for full site saturation – taken as 32.7 at/nm^2 –, X is the concentration of boron at the vicinity of austenite grain boundaries – taken as the nominal boron content –, ΔG_{seg} is the Gibbs free energy of segregation – calculated as -0.707 eV/atom at the austenitization temperature of 900 °C, k_{B} is the Boltzmann constant, and T is the temperature in Kelvin. X was taken as the nominal boron content because according to Da Rosa's model, the solubility of boron in austenite at 900 °C is 20 ppm in weight, and thus all boron is expected to be in solid solution even for the 17B steel.

Supplementary Note 9

The hardenability of low and medium alloyed steels, quantified by the critical cooling rate (g_a) to form a fully martensitic microstructure, can be estimated as[25]

$$\ln g_a = 16 - 4.62w_{\mathrm{C}} - 1.70w_{\mathrm{Mn}} + 4.00w_{\mathrm{Al}} - 0.50w_{\mathrm{Cr}} - 6.00w_{\mathrm{Mo}} - 0.54w_{\mathrm{Ni}} - 550w_{\mathrm{B}}, \quad \text{(S16)}$$

where w_i is the content in wt.% of element i and g_a is in °C/s.

Based on Eq. (S16), on the average price and equivalent CO_2 emissions to produce ferroalloys used in steelmaking, Gramlich et al.[26] compared the economic and environmental impact of adding common alloying elements with the goal of increasing the critical cooling rate by a given factor.

Supplementary Table 2. Economic and environmental impact of different elements used as alloys to increase hardenability in steels. The content of each alloying element is the content necessary to yield the same increase in hardenability as alloying the steel with 20 ppm of boron.

		Cr	Mn	Ni	Mo	B
w_i	wt. %	2.25	0.65	2.05	0.20	0.002
cost	USD/ton of steel	85.0	8.4	250	53.8	0.22
CO_2 eq.	kg/ton of steel	123	11.5	1117	203	0.22

Supplementary Note 10

The carbon enrichment of the austenite is another aspect that needs to be reevaluated when prior martensite is present, as carbon can partition from martensite to austenite. To accurately calculate the kinetics of carbon partitioning from martensite to austenite, it is necessary to solve diffusion equations for a 1, 2, or 3D representation of the microstructure. In the present work, the calculation is simplified by assuming that the kinetics of carbon partitioning from martensite follows the previously assumed kinetics of carbon partitioning from bainite.

At any time, the carbon content in the austenite can be calculated as

$$X_{\gamma} = \bar{X} + \frac{X_{\mathrm{part}}}{f_{\gamma}}, \tag{S17}$$

where X_{part} is the total carbon partitioned from bainite and martensite to austenite, and f_{γ} is the fraction of austenite.

Supplementary Figure 11 shows the calculated fraction of carbon partitioned to the austenite, X_{part}, as a function of bainite fraction for a theoretical case in which prior martensite is present. The parameters used in the calculation are given in the Figure's caption. At the beginning of the transformation, carbon partitioning is still negligible. The total carbon partitioned then increases linearly with respect to the bainite fraction, until the reaction reaches stasis. At the end of the transformation, the total fraction of carbon partitioned to austenite is $f_{\mathrm{b}}^{\mathrm{stasis}}(\bar{X} - X_{\mathrm{b}}) + f_m(\bar{X} - X_{\mathrm{m}})$, where $f_{\mathrm{b}}^{\mathrm{stasis}}$ is the fraction of

bainite at stasis – which can be calculated by combining Eq. (2) and Eq. (S17) and setting $T_0' = T$. At any point of the transformation, the carbon content in austenite can be calculated as

$$X_\gamma = \bar{X} + \frac{f_\mathrm{b}^{\mathrm{stasis}}(\bar{X} - X_\mathrm{b}) + f_\mathrm{m}(\bar{X} - X_\mathrm{m})}{1 - f_\mathrm{b} - f_\mathrm{m}} \frac{f_\mathrm{b}}{f_\mathrm{b}^{\mathrm{stasis}}}. \tag{S18}$$

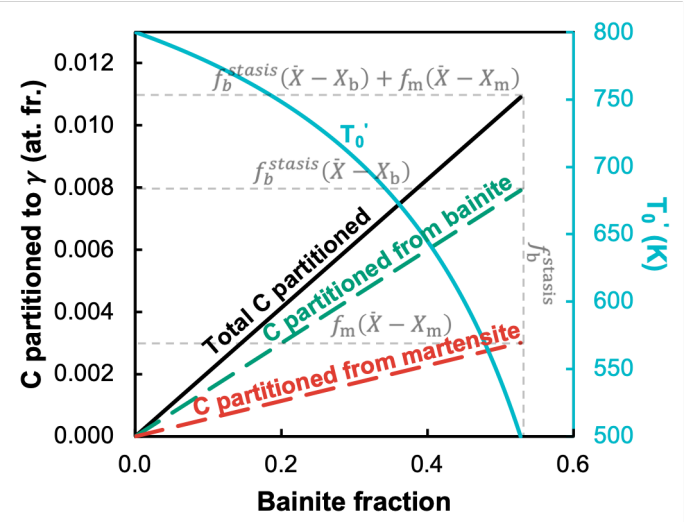

Supplementary Figure 11. Calculated curves of carbon partitioned to austenite and T_0' as a function of bainite fraction for a theoretical case. The total fraction of carbon partitioned to austenite (X_part, solid black curve) is the sum of the carbon partitioned from bainite (dashed green curve) and carbon partitioned from martensite (dashed red curve). When T_0' (solid cyan curve) reaches the temperature at which bainite is being formed, the reaction halts. The parameters used in the calculation were: $\bar{X} = 0.02$, $X_\mathrm{b} = X_\mathrm{m} = 0.005$, $f_\mathrm{m} = 0.2$, $T_{0\bar{X}}' = 800$ K, $T = 500$ K, $C_2 = 7500$ K/at. fr.

Supplementary Note 11

Autocatalysis can only start after sub-units of bainite have been formed at initially present potential nucleation sites. When martensite is present, there are two possible sites for nucleating the initial sub-units that give rise to autocatalysis: prior austenite grain boundaries and the M/A interface. Considering that $C_{\mathrm{A,AGB}}$ sub-units can form by autocatalysis from the first sub-unit formed at the AGB, and that $C_{\mathrm{A,MA}}$ sub-units can form by autocatalysis from the first sub-unit formed at the M/A interface,

$$\mathrm{d}f_{\mathrm{BA}}^{\mathrm{max}} = C_{\mathrm{A,AGB}}(1 - f_{\mathrm{BA}}^{\mathrm{max}})\mathrm{d}f_{\mathrm{GB}} + C_{\mathrm{A,MA}}(1 - f_{\mathrm{BA}}^{\mathrm{max}})\mathrm{d}f_{\mathrm{MA}}, \quad \text{(S19)}$$

with the term $(1 - f_{\mathrm{BA}}^{\mathrm{max}})$ correcting for hard impingement of bainite sheaves[16]. $C_{\mathrm{A,MA}}$ can be found by integrating Eq. (S19) considering $f_{\mathrm{AGB}} = 0$ and applying the boundary conditions that $f_{\mathrm{BA}}^{\mathrm{max}} = 0$ when no bainite has yet nucleated at the M/A interface and $f_{\mathrm{BA}}^{\mathrm{max}} = 1 - f_{\mathrm{AGB}}^{\mathrm{max}} - f_{\mathrm{MA}}^{\mathrm{max}} - f_{\mathrm{m}}$ when $f_{\mathrm{MA}} = f_{\mathrm{MA}}^{\mathrm{max}}$. The latter boundary condition states that once all the M/A interface has been consumed by bainite nucleation, all the area marked as the fraction of bainite nucleated at B/A interfaces in Figure 1b becomes available for autocatalysis, even if no bainite has nucleated at the austenite grain boundaries yet. Then, $C_{\mathrm{A,MA}}$ is found to be

$$C_{\mathrm{A,MA}} = -\frac{\ln(f_{\mathrm{AGB}}^{\mathrm{max}} + f_{\mathrm{MA}}^{\mathrm{max}} + f_{\mathrm{m}})}{f_{\mathrm{MA}}^{\mathrm{max}}}. \quad \text{(S20)}$$

The boundary conditions applied for $C_{\mathrm{A,AGB}}$ are analogous to those used for deriving $C_{\mathrm{A,MA}}$. At $f_{\mathrm{MA}} = 0$, $f_{\mathrm{BA}}^{\max} = 0$ when no bainite has nucleated at AGBs, and $f_{\mathrm{BA}}^{\max} = 1 - f_{\mathrm{AGB}}^{\max} - f_{\mathrm{MA}}^{\max} - f_{\mathrm{m}}$ when $f_{\mathrm{AGB}} = f_{\mathrm{AGB}}^{\max}$. Then, integrating Eq. (S19) and applying the proposed boundary conditions yields

$$C_{\mathrm{A,AGB}} = -\frac{\ln(f_{\mathrm{AGB}}^{\max} + f_{\mathrm{MA}}^{\max} + f_{\mathrm{m}})}{f_{\mathrm{AGB}}^{max}}. \tag{S21}$$

By integrating Eq. (S19), solving for $f_{\mathrm{BA}}^{\max}$, and including the condition that $f_{\mathrm{BA}}^{\max}$ can never be greater than $1 - f_{\mathrm{AGB}}^{\max} - f_{\mathrm{MA}}^{\max} - f_{\mathrm{m}}$, the final expression becomes Eq. (8).

The rightmost illustration in Figure 1b shows there is a region of the austenite grain in which bainite can form either by AGB or M/A nucleation. The fraction of the austenite grain that is occupied by this region can be calculated as the product $(S_{\mathrm{AGB}}u_{\mathrm{L}}) \cdot (S_{\mathrm{MA}}u_{\mathrm{L}})$, which is the extended volume of such a region (volume not counting for overlap). The relative fraction of this region that will be consumed by eacth type of nucleation depends on their relative kinetics. As we consider $n_{\mathrm{S,AGB}} = n_{\mathrm{S,MA}}$, the relative kinetics is controlled solely by the activation energies for nucleation. Using a simple weighted average, the fraction of bainite nucleated at the overlap region by nucleation at AGBs is

$$f_{\mathrm{MA}}^{\mathrm{overlap}} = (S_{\mathrm{AGB}}u_{\mathrm{L}})(S_{\mathrm{MA}}u_{\mathrm{L}})\frac{\exp\left(-\frac{Q_{\mathrm{MA}}}{RT}\right)}{\exp\left(-\frac{Q_{\mathrm{AGB}}}{RT}\right) + \exp\left(-\frac{Q_{\mathrm{MA}}}{RT}\right)}. \tag{S22}$$

By subtraction $f_{\mathrm{MA}}^{\mathrm{overlap}}$ from the extended volume for nucleation at AGB interfaces ($S_{\mathrm{AGB}}u_{\mathrm{L}}$), we arrive at Eq. (7). Following the same procedure for $f_{\mathrm{AGB}}^{\mathrm{overlap}}$, we arrive at Eq. (9).

References

1. Olson, G. B. & Cohen, M. A general mechanism of martensitic nucleation: Part III. Kinetics of martensitic nucleation. *Metall. Trans. A* **7**, 1915–1923 (1976).
2. Bhadeshia, H. K. D. H. *Bainite in Steels: Theory and Practice, Third Edition*. (CRC Press, London, 2015). doi:10.1201/9781315096674.
3. Raghavan, V. Formation sequence of plates in isothermal martensite transformation. *Acta Metall.* **17**, 1299–1303 (1969).
4. McMurtrie, D. G. & Magee, C. L. The average volume of martensite plates during transformation. *Metall. Trans.* **1**, 3185–3191 (1970).
5. Nambu, S. *et al.* In situ observations and crystallographic analysis of martensitic transformation in steel. *Acta Mater.* **61**, 4831–4839 (2013).
6. Galindo-Nava, E. I. & Rivera-Díaz-del-Castillo, P. E. J. A model for the microstructure behaviour and strength evolution in lath martensite. *Acta Mater.* **98**, 81–93 (2015).
7. Koistinen, D. P. & Marburger, R. E. A general equation prescribing the extent of the austenite-martensite transformation in pure iron-carbon alloys and plain carbon steels. *Acta Metall.* **7**, 59–60 (1959).
8. van Bohemen, S. M. C. Bainite and martensite start temperature calculated with exponential carbon dependence. *Mater. Sci. Technol.* **28**, 487–495 (2012).
9. C. L. Magee. The nucleation of martensite. in *Phase Transformations* 115–156 (ASM, 1970).
10. Khan, S. A. & Bhadeshia, H. K. D. Kinetics of Martensitic transformation in partially bainitic 300M steel. *Mater. Sci. Eng. A* **129**, 257–272 (1990).

11. Huyan, F., Hedström, P., Höglund, L. & Borgenstam, A. A Thermodynamic-Based Model to Predict the Fraction of Martensite in Steels. *Metall. Mater. Trans. A* **47**, 4404–4410 (2016).

12. Raghavan, V. & Entwisle, A. R. Isothermal martensite kinetics in iron alloys. in *Physical Properties of Martensite and Bainite* 30–37 (Iron and Steel Institute, 1965).

13. Pati, S. R. & Cohen, M. Nucleation of the isothermal martensitic transformation. *Acta Metall.* **17**, 189–199 (1969).

14. Smanio, V. & Sourmail, T. Effect of Partial Martensite Transformation on Bainite Reaction Kinetics in Different 1%C Steels. *Solid State Phenom.* **172–174**, 821–826 (2011).

15. Ribamar, G. G. *et al.* Austenite carbon enrichment and decomposition during quenching and tempering of high silicon high carbon bearing steel. *Acta Mater.* **247**, 118742 (2023).

16. Avila, D. dos S., Offerman, S. E. & Santofimia, M. J. Modeling the effect of prior austenite grain size on bainite formation kinetics. *Acta Mater.* **266**, 119656 (2024).

17. Prithiv, T. S. *et al.* Austenite grain boundary segregation and precipitation of boron in low-C steels and their role on the heterogeneous nucleation of ferrite. *Acta Mater.* **252**, 118947 (2023).

18. Hachet, G. *et al.* Segregation at prior austenite grain boundaries: The competition between boron and hydrogen. *Int. J. Hydrog. Energy* **95**, 734–746 (2024).

19. Navarro-López, A., Sietsma, J. & Santofimia, M. J. Effect of Prior Athermal Martensite on the Isothermal Transformation Kinetics Below Ms in a Low-C High-Si Steel. *Metall. Mater. Trans. A* **47**, 1028–1039 (2016).

20. van Bohemen, S. M. C. & Sietsma, J. Kinetics of martensite formation in plain carbon steels: critical assessment of possible influence of austenite grain boundaries and autocatalysis. *Mater. Sci. Technol.* **30**, 1024–1033 (2014).

21. Catteau, S. D., Sourmail, T. & Moine, A. Dilatometric Study of Phase Transformations in Steels: Some Issues. *Mater. Perform. Charact.* **5**, 564–584 (2016).

22. Ravi, A. M., Navarro-López, A., Sietsma, J. & Santofimia, M. J. Influence of martensite/austenite interfaces on bainite formation in low-alloy steels below *Ms*. *Acta Mater.* **188**, 394–405 (2020).

23. Da Rosa, G. *et al*. Grain-boundary segregation of boron in high-strength steel studied by nano-SIMS and atom probe tomography. *Acta Mater.* **182**, 226–234 (2020).

24. McLean, D. & Maradudin, A. Grain Boundaries in Metals. *Phys. Today* **11**, 35–36 (1958).

25. Gramlich, A., van der Linde, C., Ackermann, M. & Bleck, W. Effect of molybdenum, aluminium and boron on the phase transformation in 4 wt.–% manganese steels. *Results Mater.* **8**, 100147 (2020).

26. Gramlich, A., Helbig, C., Schmidt, M. & Hagedorn, W. A comprehensive design approach to increase the performance of steels under minimal costs and environmental impacts. *Sustain. Mater. Technol.* **41**, e01040 (2024).